# Single vector boson production in $e^+e^-$ collisions at centre-of-mass energies from 183 to 209 GeV

S. Schael, R. Barate, R. Bruneliere, I. de Bonis, D. Decamp, C. Goy, S. Jezequel, J P. Lees, F. Martin, E. Merle, et al.

EUROPEAN ORGANIZATION FOR NUCLEAR RESEARCH (CERN)

CERN-PH-EP/2004-034
July 26, 2004

# Single vector boson production in $e^+e^-$ collisions at centre-of-mass energies from 183 to 209 GeV

The ALEPH Collaboration*)

**Abstract**

The cross sections for single vector boson production in the We$\nu$ and Zee channels are measured from the data collected by the ALEPH detector at LEP for centre-of-mass energies between 183 and 209 GeV. These data correspond to a total integrated luminosity of 683 $\mathrm{pb}^{-1}$. Single-W production is studied in both hadronic and leptonic decay channels. Hadronic and dimuon decays are used for single-Z production. The measured cross sections agree with the Standard Model predictions.

*Submitted to Physics Letter B*

---

*) See next pages for the list of authors

# The ALEPH Collaboration

S. Schael

*Physikalisches Institut das RWTH-Aachen, D-52056 Aachen, Germany*

R. Barate, R. Brunelière, I. De Bonis, D. Decamp, C. Goy, S. Jézéquel, J.-P. Lees, F. Martin, E. Merle, M.-N. Minard, B. Pietrzyk, B. Trocmé

*Laboratoire de Physique des Particules (LAPP), IN$^2$P$^3$-CNRS, F-74019 Annecy-le-Vieux Cedex, France*

S. Bravo, M.P. Casado, M. Chmeissani, J.M. Crespo, E. Fernandez, M. Fernandez-Bosman, Ll. Garrido,[15] M. Martinez, A. Pacheco, H. Ruiz

*Institut de Física d'Altes Energies, Universitat Autònoma de Barcelona, E-08193 Bellaterra (Barcelona), Spain*[7]

A. Colaleo, D. Creanza, N. De Filippis, M. de Palma, G. Iaselli, G. Maggi, M. Maggi, S. Nuzzo, A. Ranieri, G. Raso,[24] F. Ruggieri, G. Selvaggi, L. Silvestris, P. Tempesta, A. Tricomi,[3] G. Zito

*Dipartimento di Fisica, INFN Sezione di Bari, I-70126 Bari, Italy*

X. Huang, J. Lin, Q. Ouyang, T. Wang, Y. Xie, R. Xu, S. Xue, J. Zhang, L. Zhang, W. Zhao

*Institute of High Energy Physics, Academia Sinica, Beijing, The People's Republic of China*[8]

D. Abbaneo, T. Barklow,[26] O. Buchmüller,[26] M. Cattaneo, B. Clerbaux,[23] H. Drevermann, R.W. Forty, M. Frank, F. Gianotti, J.B. Hansen, J. Harvey, D.E. Hutchcroft,[30], P. Janot, B. Jost, M. Kado,[2] P. Mato, A. Moutoussi, F. Ranjard, L. Rolandi, D. Schlatter, G. Sguazzoni, F. Teubert, A. Valassi, I. Videau

*European Laboratory for Particle Physics (CERN), CH-1211 Geneva 23, Switzerland*

F. Badaud, S. Dessagne, A. Falvard,[20] D. Fayolle, P. Gay, J. Jousset, B. Michel, S. Monteil, D. Pallin, J.M. Pascolo, P. Perret

*Laboratoire de Physique Corpusculaire, Université Blaise Pascal, IN$^2$P$^3$-CNRS, Clermont-Ferrand, F-63177 Aubière, France*

J.D. Hansen, J.R. Hansen, P.H. Hansen, A.C. Kraan, B.S. Nilsson

*Niels Bohr Institute, 2100 Copenhagen, DK-Denmark*[9]

A. Kyriakis, C. Markou, E. Simopoulou, A. Vayaki, K. Zachariadou

*Nuclear Research Center Demokritos (NRCD), GR-15310 Attiki, Greece*

A. Blondel,[12] J.-C. Brient, F. Machefert, A. Rougé, H. Videau

*Laoratoire Leprince-Ringuet, Ecole Polytechnique, IN$^2$P$^3$-CNRS, F-91128 Palaiseau Cedex, France*

V. Ciulli, E. Focardi, G. Parrini

*Dipartimento di Fisica, Università di Firenze, INFN Sezione di Firenze, I-50125 Firenze, Italy*

A. Antonelli, M. Antonelli, G. Bencivenni, F. Bossi, G. Capon, F. Cerutti, V. Chiarella, P. Laurelli, G. Mannocchi,[5] G.P. Murtas, L. Passalacqua

*Laboratori Nazionali dell'INFN (LNF-INFN), I-00044 Frascati, Italy*

J. Kennedy, J.G. Lynch, P. Negus, V. O'Shea, A.S. Thompson

*Department of Physics and Astronomy, University of Glasgow, Glasgow G12 8QQ,United Kingdom*[10]

S. Wasserbaech

*Utah Valley State College, Orem, UT 84058, U.S.A.*

R. Cavanaugh,[4] S. Dhamotharan,[21] C. Geweniger, P. Hanke, V. Hepp, E.E. Kluge, A. Putzer, H. Stenzel, K. Tittel, M. Wunsch[19]

*Kirchhoff-Institut für Physik, Universität Heidelberg, D-69120 Heidelberg, Germany*[16]

R. Beuselinck, W. Cameron, G. Davies, P.J. Dornan, M. Girone,[1] N. Marinelli, J. Nowell, S.A. Rutherford, J.K. Sedgbeer, J.C. Thompson,[14] R. White

*Department of Physics, Imperial College, London SW7 2BZ, United Kingdom*[10]

V.M. Ghete, P. Girtler, E. Kneringer, D. Kuhn, G. Rudolph

*Institut für Experimentalphysik, Universität Innsbruck, A-6020 Innsbruck, Austria*[18]

E. Bouhova-Thacker, C.K. Bowdery, D.P. Clarke, G. Ellis, A.J. Finch, F. Foster, G. Hughes, R.W.L. Jones, M.R. Pearson, N.A. Robertson, M. Smizanska

*Department of Physics, University of Lancaster, Lancaster LA1 4YB, United Kingdom*[10]

O. van der Aa, C. Delaere,[28] G.Leibenguth,[31] V. Lemaitre[29]

*Institut de Physique Nucléaire, Département de Physique, Université Catholique de Louvain, 1348 Louvain-la-Neuve, Belgium*

U. Blumenschein, F. Hölldorfer, K. Jakobs, F. Kayser, K. Kleinknecht, A.-S. Müller, B. Renk, H.-G. Sander, S. Schmeling, H. Wachsmuth, C. Zeitnitz, T. Ziegler

*Institut für Physik, Universität Mainz, D-55099 Mainz, Germany*[16]

A. Bonissent, P. Coyle, C. Curtil, A. Ealet, D. Fouchez, P. Payre, A. Tilquin

*Centre de Physique des Particules de Marseille, Univ Méditerranée, IN$^2$P$^3$-CNRS, F-13288 Marseille, France*

F. Ragusa

*Dipartimento di Fisica, Università di Milano e INFN Sezione di Milano, I-20133 Milano, Italy.*

A. David, H. Dietl,[32] G. Ganis,[27] K. Hüttmann, G. Lütjens, W. Männer[32], H.-G. Moser, R. Settles, M. Villegas, G. Wolf

*Max-Planck-Institut für Physik, Werner-Heisenberg-Institut, D-80805 München, Germany*[16]

J. Boucrot, O. Callot, M. Davier, L. Duflot, J.-F. Grivaz, Ph. Heusse, A. Jacholkowska,[6] L. Serin, J.-J. Veillet

*Laboratoire de l'Accélérateur Linéaire, Université de Paris-Sud, IN$^2$P$^3$-CNRS, F-91898 Orsay Cedex, France*

P. Azzurri, G. Bagliesi, T. Boccali, L. Foà, A. Giammanco, A. Giassi, F. Ligabue, A. Messineo, F. Palla, G. Sanguinetti, A. Sciabà, P. Spagnolo, R. Tenchini, A. Venturi, P.G. Verdini

*Dipartimento di Fisica dell'Università, INFN Sezione di Pisa, e Scuola Normale Superiore, I-56010 Pisa, Italy*

O. Awunor, G.A. Blair, G. Cowan, A. Garcia-Bellido, M.G. Green, T. Medcalf, A. Misiejuk, J.A. Strong, P. Teixeira-Dias

*Department of Physics, Royal Holloway & Bedford New College, University of London, Egham, Surrey TW20 OEX, United Kingdom*[10]

R.W. Clifft, T.R. Edgecock, P.R. Norton, I.R. Tomalin, J.J. Ward

*Particle Physics Dept., Rutherford Appleton Laboratory, Chilton, Didcot, Oxon OX11 OQX, United Kingdom*[10]

B. Bloch-Devaux, D. Boumediene, P. Colas, B. Fabbro, E. Lançon, M.-C. Lemaire, E. Locci, P. Perez, J. Rander, B. Tuchming, B. Vallage

*CEA, DAPNIA/Service de Physique des Particules, CE-Saclay, F-91191 Gif-sur-Yvette Cedex, France*[17]

A.M. Litke, G. Taylor

*Institute for Particle Physics, University of California at Santa Cruz, Santa Cruz, CA 95064, USA*[22]

C.N. Booth, S. Cartwright, F. Combley,[25] P.N. Hodgson, M. Lehto, L.F. Thompson

*Department of Physics, University of Sheffield, Sheffield S3 7RH, United Kingdom*[10]

A. Böhrer, S. Brandt, C. Grupen, J. Hess, A. Ngac, G. Prange

*Fachbereich Physik, Universität Siegen, D-57068 Siegen, Germany*[16]

C. Borean, G. Giannini

*Dipartimento di Fisica, Università di Trieste e INFN Sezione di Trieste, I-34127 Trieste, Italy*

H. He, J. Putz, J. Rothberg

*Experimental Elementary Particle Physics, University of Washington, Seattle, WA 98195 U.S.A.*

S.R. Armstrong, K. Berkelman, K. Cranmer, D.P.S. Ferguson, Y. Gao,[13] S. González, O.J. Hayes, H. Hu, S. Jin, J. Kile, P.A. McNamara III, J. Nielsen, Y.B. Pan, J.H. von Wimmersperg-Toeller, W. Wiedenmann, J. Wu, Sau Lan Wu, X. Wu, G. Zobernig

*Department of Physics, University of Wisconsin, Madison, WI 53706, USA*[11]

G. Dissertori

*Institute for Particle Physics, ETH Hönggerberg, 8093 Zürich, Switzerland.*

---

[1]Also at CERN, 1211 Geneva 23, Switzerland.

[2]Now at Fermilab, PO Box 500, MS 352, Batavia, IL 60510, USA

[3]Also at Dipartimento di Fisica di Catania and INFN Sezione di Catania, 95129 Catania, Italy.

[4]Now at University of Florida, Department of Physics, Gainesville, Florida 32611-8440, USA

[5]Also IFSI sezione di Torino, CNR, Italy.

[6]Also at Groupe d'Astroparticules de Montpellier, Université de Montpellier II, 34095, Montpellier, France.

[7]Supported by CICYT, Spain.

[8]Supported by the National Science Foundation of China.

[9]Supported by the Danish Natural Science Research Council.

[10]Supported by the UK Particle Physics and Astronomy Research Council.

[11]Supported by the US Department of Energy, grant DE-FG0295-ER40896.

[12]Now at Departement de Physique Corpusculaire, Université de Genève, 1211 Genève 4, Switzerland.

[13]Also at Department of Physics, Tsinghua University, Beijing, The People's Republic of China.

[14]Supported by the Leverhulme Trust.

[15]Permanent address: Universitat de Barcelona, 08208 Barcelona, Spain.

[16]Supported by Bundesministerium für Bildung und Forschung, Germany.

[17]Supported by the Direction des Sciences de la Matière, C.E.A.

[18]Supported by the Austrian Ministry for Science and Transport.

[19]Now at SAP AG, 69185 Walldorf, Germany

[20]Now at Groupe d' Astroparticules de Montpellier, Université de Montpellier II, 34095 Montpellier, France.

[21]Now at BNP Paribas, 60325 Frankfurt am Mainz, Germany

[22]Supported by the US Department of Energy, grant DE-FG03-92ER40689.

[23]Now at Institut Inter-universitaire des hautes Energies (IIHE), CP 230, Université Libre de Bruxelles, 1050 Bruxelles, Belgique

[24]Now at Dipartimento di Fisica e Tecnologie Relative, Università di Palermo, Palermo, Italy.

[25]Deceased.

[26]Now at SLAC, Stanford, CA 94309, U.S.A

[27]Now at CERN, 1211 Geneva 23, Switzerland

[28]Research Fellow of the Belgium FNRS

[29]Research Associate of the Belgium FNRS

[30]Now at Liverpool University, Liverpool L69 7ZE, United Kingdom

[31]Supported by the Federal Office for Scientific, Technical and Cultural Affairs through the Interuniversity Attraction Pole P5/27

[32]Now at Henryk Niewodniczanski Institute of Nuclear Physics, Polish Academy of Sciences, Cracow, Poland

# 1 Introduction

In this letter a measurement of single vector boson production with the processes $e^+e^- \to We\nu$ and Zee (called in the following single-W and single-Z) is described. The data were collected at LEP by the ALEPH detector at centre-of-mass (CM) energies between 183 and 209 GeV and correspond to an integrated luminosity of 683 $pb^{-1}$. The breakdown of CM energies and luminosities is given in Table 1.

Table 1: Summary of the CM energies and integrated luminosities.

| Sample Name | Average CM energy (GeV) | Luminosity ($pb^{-1}$) |
|---|---|---|
| 183 | 182.65 | 56.8 ± 0.3 |
| 189 | 188.63 | 174.2 ± 0.8 |
| 192 | 191.58 | 28.9 ± 0.1 |
| 196 | 195.52 | 79.9 ± 0.4 |
| 200 | 199.52 | 86.3 ± 0.4 |
| 202 | 201.62 | 41.9 ± 0.2 |
| 205 | 204.86 | 81.4 ± 0.4 |
| 207 | 206.53 | 133.2 ± 0.6 |

At LEP2 energies, the single vector boson production cross section is of the order of 1 pb [1], i.e., a few percent of the dominant Z and W resonant production, $e^+e^- \to Z\gamma$ ($\sigma \sim 100$ pb) and $W^+W^-$ ($\sigma \sim 18$ pb). Single-W and single-Z production provides, however, significant background for many searches at LEP. A direct measurement of these processes is therefore an important cross-check of Standard Model predictions. The single-W process is also of interest because it probes the triple gauge $WW\gamma$ coupling [2] with a sensitivity complementary to that of WW production.

All W decay modes are reconstructed in the analysis presented here. The $We\nu$ cross-section measurement is performed separately for the leptonic and the hadronic channels at each CM energy. Two decay channels, $Z \to \mu^+\mu^-$ and $Z \to q\bar{q}$, are used for the single-Z cross-section measurement. Because this cross section varies by only 5% over the LEP2 energy range, the measurement in the dimuon channel is averaged over the whole energy range. The higher hadronic cross section allows a significant measurement to be made at each CM energy.

# 2 The ALEPH detector

A detailed description of the ALEPH detector can be found in Ref. [3] and of its performance in Ref. [4]. Charged particles are detected in the central part, which consists of a precision silicon vertex detector (VDET), a cylindrical drift chamber (ITC) and a large time projection chamber (TPC), together measuring up to 31 space points along the charged particle trajectories. A 1.5 T axial magnetic field is provided by a superconducting solenoid. Charged-particle transverse momenta are reconstructed with a $1/p_T$ resolution

of $(6 \times 10^{-4} \oplus 5 \times 10^{-3}/p_{\mathrm{T}})$ $(\mathrm{GeV}/c)^{-1}$. The tracks used in the present analysis are reconstructed with at least four hits in the TPC and originate from within a cylinder of length 20 cm and radius 2 cm coaxial with the beam, centred at the nominal collision point.

In addition to its rôle as a tracking device, the TPC also measures the specific energy loss by ionization, $\mathrm{d}E/\mathrm{d}x$. It allows low momentum electrons to be separated from other charged particle species by more than three standard deviations up to a momentum of $8\,\mathrm{GeV}/c$.

Electrons (and photons) are also identified by the characteristic longitudinal and transverse development of the associated showers in the electromagnetic calorimeter (ECAL), a 22 radiation-length-thick sandwich of lead planes and proportional wire chambers with fine read-out segmentation. A relative energy resolution of $0.18/\sqrt{E}$ ($E$ in GeV) is achieved for isolated electrons and photons.

Muons are identified by their characteristic penetration pattern in the hadron calorimeter (HCAL), a 1.2 m thick iron yoke interleaved with 23 layers of streamer tubes, together with two surrounding double-layers of muon chambers. In association with the electromagnetic calorimeter, the hadron calorimeter also provides a measurement of the hadronic energy with a relative resolution of $0.85/\sqrt{E}$ ($E$ in GeV). The specific algorithms used for lepton identification are described in Ref. [5].

The total visible energy is measured with an energy-flow reconstruction algorithm which combines all the above measurements [4]. The relative resolution on the total visible energy is $0.60/\sqrt{E}$ ($E$ in GeV) for high multiplicity final states. In addition to the visible-energy measurement, the energy-flow reconstruction algorithm also provides a list of reconstructed objects, classified as charged particles, photons and neutral hadrons, and called *energy-flow objects* in the following. Unless otherwise specified, these energy-flow objects are the basic entities used in the present analysis.

Down to 34 mrad from the beam axis, the acceptance is closed at both ends of the experiment by the luminosity calorimeter (LCAL) [6] and a tungsten-silicon calorimeter (SICAL) [7] originally designed for the LEP1 luminosity measurement. The dead regions between the two LCAL modules at each end are covered by pairs of scintillators. The luminosity is measured with small-angle Bhabha events with the LCAL with an uncertainty less than 0.5%.

The trigger system plays an important rôle in the detection of single vector boson events, particularly for single-W leptonic decays to electrons or muons with a single track in the detector acceptance. The relevant trigger for a single electron requires a track segment in the ITC to be in spatial coincidence with an energy deposit in the module of the ECAL to which the track is pointing. The energy threshold in ECAL is set to 1.0 GeV in the barrel and 1.2 GeV in the endcap region. For single muons, an ITC-HCAL coincidence is required, with at least four out of twelve double planes of HCAL tubes fired in the same azimuthal region as the ITC track segment. The trigger efficiency for selected single-W events is measured with simulated events to be 96.1% for single muons and 99.3% for single electrons. The combination of these and other calorimetric trigger conditions yields an efficiency of 99.3% for single taus.

In this letter, the polar angle $\theta$ is the angle with respect to the incoming electron beam direction.

# 3 Signal and background simulation

## 3.1 Single-W signal definition

The dominant diagrams contributing to the single-W hadronic final states are shown in Fig. 1a. To evaluate the selection efficiency, the signal definition adopted here is based on the full set of four-fermion diagrams compatible with the We$\nu$ final states. The following additional cuts are included in the definition.

- One electron (positron) must be produced with an angle with respect to the beam axis smaller than 34 mrad.
- For W leptonic decays, the lepton must have an energy in excess of 20 GeV and a $|\cos\theta|$ value smaller than 0.95.
- For W hadronic decays, the hadronic invariant mass must be larger than 60 GeV/$c^2$.

In the following, the four-fermion events compatible with a WW final state but not fulfilling the single-W signal definition are called WW events. (Different definitions have been used by other LEP experiments; for the definition used by the LEP Electroweak Working Group [8], the measured cross sections given in this letter have to be scaled by a factor $1.50 \pm 0.03$ to be combined with the other LEP results.)

## 3.2 Single-Z signal definition

In the Zee process, one of the two electrons has radiated a quasi-real photon and is usually lost along the beam axis while the second is in general within the detector acceptance together with the Z decay products. The main diagrams describing this process are shown in Fig. 1b. The signal definition is based on the set of four-fermion diagrams compatible with an $e^+e^-f\bar{f}$ final state (f=q or $\mu$) with the following additional cuts.

- The difermion invariant mass must exceed 60 GeV/$c^2$.
- The polar angle of the low angle electron (positron) must be smaller than 12° (larger than 168°).
- The energy of the large angle positron (electron) must exceed 3 GeV and its polar angle must be between 12° and 120° (60° and 168°).

The NC8 diagrams [8] with two electrons in the final state (such as $e^+e^- \to ZZ$ with one of the Z's decaying to $e^+e^-$) and the two-photon processes contribute to the signal definition. (This definition coincides with that used by the LEP Electroweak Working Group.)

## 3.3 Signal and background event generators

Single-W and single-Z events were generated with the `KoralW` generator [9]. The selection efficiency determined by `KoralW` was found to agree with that predicted by `GRC4F` (single-W) [10] within 3% and `PYTHIA` (single-Z) [11] within 2%. The residual difference

is quoted in Sections 4 and 5 as a generator-dependent efficiency systematic uncertainty. An additional theoretical uncertainty of 5% affects the cross section of all four-fermion event generators [8].

The background contamination is determined as in Ref. [5]. The signal and background simulation was performed at all CM energies of Table 1.

# 4 Single-W production

## 4.1 Event selection

### 4.1.1 Leptonic selection

Leptonic single-W events are characterized by either single electron/muon track or a low multiplicity jet from a tau decay within the detector acceptance. As a consequence, only events with one or three tracks with $|\cos\theta| < 0.95$ are kept. If the single charged particle fulfils the electron or muon identification criteria, the event is classified as e$\nu$ or $\mu\nu$. The remaining events are considered as $\tau\nu$ candidates. Further cuts are applied on the transverse missing momentum ($p_{\mathrm{T}}^{\mathrm{miss}}/\sqrt{s}$ >0.06) and the total invariant mass ($M_{\mathrm{vis}} < 5\,\mathrm{GeV}/c^2$). The momentum of the reconstructed electron/muon, corrected for possible bremsstrahlung emission as in Ref. [5], must be greater than $20\,\mathrm{GeV}/c$. No energy should be measured within a 14° cone around the beam axis. This requirement removes most of the $\gamma\gamma$ background. Because of this cut, beam-gas interactions, off-momentum beam particles or detector noise (not modelled in the simulation) lead to an overall 2% inefficiency evaluated from events triggered at random beam crossings as in Ref. [5].

The lepton transverse-momentum ($p_{\mathrm{T}}^{\ell}$) distributions for the three lepton types with the contributions of signal and various background simulations are shown in Fig. 2. The average efficiencies are given in Table 2 for the three leptonic channels. The breakdown of the numbers of events selected and the signal and background events expected is given in Table 3 at each CM energy. The Zee process contributes 60% of the remaining background. A total of 102 events is selected in the data.

Table 2: Lepton selection efficiencies and cross-channel contaminations for We$\nu$, averaged over all CM energies. The statistical precision is 0.2% for the diagonal terms and less than 0.1% for the non-diagonal ones.

| | | Event classification | | |
|---|---|---|---|---|
| | | e$\nu$ | $\mu\nu$ | $\tau\nu$ |
| Efficiency (%) | W $\to$ e$\nu$ | 69.4 | 0.0 | 1.1 |
| | W $\to \mu\nu$ | 0.0 | 72.6 | 1.0 |
| | W $\to \tau\nu$ | 7.4 | 5.2 | 28.5 |

Table 3: Numbers of selected events in the single-W leptonic and hadronic channels and expected background contaminations for each CM energy. The quoted errors are due to the finite statistics of the simulation.

| | Leptonic | | | Hadronic | | |
|---|---|---|---|---|---|---|
| Energy (GeV) | Selected events | Expected signal | Expected background | Selected events | Expected signal | Expected background |
| 183 | 7 | $4.7 \pm 0.1$ | $3.3 \pm 0.1$ | 11 | $4.9 \pm 0.1$ | $5.5 \pm 0.1$ |
| 189 | 25 | $15.7 \pm 0.1$ | $9.9 \pm 0.3$ | 40 | $18.3 \pm 0.2$ | $26.2 \pm 0.2$ |
| 192 | 6 | $2.7 \pm 0.1$ | $1.6 \pm 0.1$ | 6 | $2.5 \pm 0.1$ | $3.2 \pm 0.1$ |
| 196 | 13 | $8.2 \pm 0.1$ | $4.8 \pm 0.1$ | 22 | $8.9 \pm 0.1$ | $11.2 \pm 0.1$ |
| 200 | 14 | $9.4 \pm 0.1$ | $5.2 \pm 0.2$ | 38 | $11.8 \pm 0.1$ | $15.0 \pm 0.1$ |
| 202 | 4 | $4.8 \pm 0.1$ | $2.7 \pm 0.1$ | 16 | $6.2 \pm 0.1$ | $8.0 \pm 0.1$ |
| 205 | 15 | $9.7 \pm 0.1$ | $4.9 \pm 0.2$ | 23 | $12.7 \pm 0.1$ | $15.8 \pm 0.2$ |
| 207 | 18 | $16.4 \pm 0.1$ | $8.6 \pm 0.3$ | 49 | $21.8 \pm 0.2$ | $26.3 \pm 0.3$ |
| Total | 102 | $71.7 \pm 0.3$ | $40.8 \pm 0.5$ | 205 | $87.1 \pm 0.3$ | $111.2 \pm 0.4$ |

#### 4.1.2 Hadronic selection

The topology of hadronic single-W events is characterized by two jets in the detector acceptance. Events are accepted if they contain at least seven tracks carrying more than 10% of the CM energy and if the missing momentum polar angle satisfies $|\cos\theta_{\rm miss}| < 0.9$. Two hemispheres are defined with respect to a plane perpendicular to the thrust axis. The acollinearity angle between the sum of the energy-flow objects momenta in the two hemispheres is required to be smaller than 165°. The visible mass $M_{\rm vis}$ is required to be larger than $40\,\mathrm{GeV}/c^2$. These cuts are applied to reject difermion and two-photon backgrounds. Events including an identified electron or muon with an energy larger than 5% of the CM energy are rejected. The energy observed below 14° of the beam axis is required to be smaller than 2.5% of the CM energy which induces a 1% efficiency loss. In addition, events already identified as WW events [5] are rejected.

The last step of the selection is based on a neural network trained with the following variables.

- Event variables: thrust, sphericity, visible energy $E_{\rm vis}$, visible mass $M_{\rm vis}$, missing transverse momentum $p_{\rm T}^{\rm miss}$, acollinearity and acoplanarity.

- Tau variables: in the presence of a one- or three-prong jet (reconstructed with the `JADE` [12] algorithm with $y_{\rm cut} = 0.001$) with an energy $E_{\rm ch}$ carried by charged particles larger than 2.5% of the CM energy, its total energy and $E_{\rm ch}$ are also inputs to the neural network computation.

Events are selected by cutting on the neural network output. The cut value is chosen to maximize the product of the efficiency and the purity [5].

Figure 3 displays the reconstructed W transverse momentum ($p_{\rm T}^{\rm W}$) distribution of the selected events with the contributions from signal and various background simulations. The average signal efficiency is $(38.1 \pm 0.1)\%$. The breakdown of the numbers of events

selected and the signal and background events expected are listed in Table 3 for each CM energy. The semileptonic WW$\rightarrow$ $q'\bar{q}\tau\nu$ and ZZ events contribute 54% and 41% of the remaining background, respectively. In the data, 205 events are selected.

## 4.2 Single-W cross section results

The systematic uncertainties related to detector simulation, background contamination (except WW), beam-related background, luminosity determination, hadronization and lepton identification are evaluated as for the W-pair cross section measurement [5]. The generator-dependent efficiency uncertainty is mentioned in Section 3. Other sources are listed in the following paragraphs.

### WW contamination

An uncertainty of 0.5% is assigned to the WW cross-section [5] and is propagated to the background contamination rate.

### Simulated statistics

The finite simulated statistics yield a 2% uncertainty at each CM energy. For the leptonic channel, this uncertainty is dominated by the limited number of generated Zee events. The uncertainty on the hadronic channel is caused by to the WW sample size.

### Trigger simulation

The trigger efficiency for the leptonic channels was monitored with dilepton events. A conservative uncertainty of 0.5% is assigned to the trigger efficiency computed with simulated events.

A summary of all systematic uncertainties is given in Table 4.

Table 4: Single-W cross section systematic uncertainty contributions for hadronic and leptonic channels, at each CM energy.

| | Relative uncertainty in % | |
|---|---|---|
| Source | Leptonic | Hadronic |
| Generator-dependent efficiency | 3.0 | 3.0 |
| Simulated statistics | 2.0 | 2.0 |
| Detector simulation | 0.7 | 2.1 |
| Background contamination | 1.5 | 1.1 |
| Beam-related background | 0.7 | 1.1 |
| Luminosity determination | 0.7 | 1.1 |
| Hadronization | - | 1.0 |
| Trigger simulation | 0.2 | - |
| Lepton identification | $<0.1$ | - |
| Total | 4.1 | 4.7 |

The leptonic cross section is computed from the total number of selected events, corrected for the efficiency sum in the three channels. (This procedure is based on the assumption of lepton universality). The leptonic and hadronic cross section measured values are given in Table 5 for each CM energy. The sum (the total We$\nu$ cross section) is compared to the GRC4F generator prediction in Table 6 and Fig. 4.

Table 5: Measured leptonic ($\sigma_{\rm lep}$) and hadronic ($\sigma_{\rm had}$) single-W cross sections for each CM energy.

| Energy (GeV) | $\sigma_{\rm lep} \pm$ stat. $\pm$ syst. (pb) | $\sigma_{\rm had} \pm$ stat. $\pm$ syst. (pb) |
|---|---|---|
| 183 | $0.11 \pm 0.08 \pm 0.01$ | $0.30 \pm 0.18 \pm 0.01$ |
| 189 | $0.14 \pm 0.05 \pm 0.01$ | $0.22 \pm 0.10 \pm 0.01$ |
| 192 | $0.25 \pm 0.14 \pm 0.01$ | $0.35 \pm 0.31 \pm 0.01$ |
| 196 | $0.17 \pm 0.07 \pm 0.01$ | $0.41 \pm 0.18 \pm 0.01$ |
| 200 | $0.17 \pm 0.07 \pm 0.01$ | $0.70 \pm 0.19 \pm 0.02$ |
| 202 | $0.05 \pm 0.08 \pm 0.01$ | $0.48 \pm 0.24 \pm 0.02$ |
| 205 | $0.21 \pm 0.08 \pm 0.01$ | $0.22 \pm 0.15 \pm 0.02$ |
| 207 | $0.12 \pm 0.05 \pm 0.01$ | $0.42 \pm 0.13 \pm 0.02$ |

Table 6: Measured single-W cross section and expected uncertainty for each CM energy. In the second column, the ratio between the measured cross section and that predicted by GRC4F ($\rm R_W$) is given.

| Energy (GeV) | $\sigma \pm$ stat. $\pm$ syst. (pb) | $\rm R_W \pm$ stat. $\pm$ syst. |
|---|---|---|
| 183 | $0.40 \pm 0.19 \pm 0.02$ | $0.97 \pm 0.46 \pm 0.04$ |
| 189 | $0.36 \pm 0.12 \pm 0.02$ | $0.78 \pm 0.25 \pm 0.04$ |
| 192 | $0.60 \pm 0.32 \pm 0.02$ | $1.21 \pm 0.65 \pm 0.04$ |
| 196 | $0.58 \pm 0.18 \pm 0.02$ | $1.10 \pm 0.35 \pm 0.04$ |
| 200 | $0.87 \pm 0.17 \pm 0.02$ | $1.55 \pm 0.31 \pm 0.04$ |
| 202 | $0.53 \pm 0.25 \pm 0.02$ | $0.92 \pm 0.43 \pm 0.04$ |
| 205 | $0.43 \pm 0.18 \pm 0.03$ | $0.71 \pm 0.30 \pm 0.04$ |
| 207 | $0.54 \pm 0.14 \pm 0.03$ | $0.86 \pm 0.23 \pm 0.04$ |

The average ratio of the measured cross section to that predicted by GRC4F is :

$$\rm R_W = 0.96 \pm 0.11(stat.) \pm 0.04(syst.).$$

As a cross-check, the same ratio was computed with KoralW and amounts to $1.00 \pm 0.12$(stat.) $\pm 0.04$(syst.).

# 5 Single-Z production

## 5.1 Event selection

### 5.1.1 Dimuon events

A single-Z dimuon event is characterized by a soft isolated electron at large angle, large missing momentum along the beam direction and a $Z \to \mu^+\mu^-$ decay within the detector acceptance. Events are required to have exactly three tracks with a momentum greater than $1\,\mathrm{GeV}/c$ and reconstructed with at least one VDET hit. The total electric charge must equal $\pm 1$. At least two of the three tracks are required to be identified as electron or muon, and their flavours and electric charges must be consistent with the $\mu^+\mu^-e^\pm$ final state. If only two tracks are identified, the flavour of the third is inferred from the first two. The momentum of the reconstructed electron (positron) is corrected for possible bremsstrahlung emission as in Ref. [13]. The selection requirements include all the cuts listed in the signal definition and two additional angular cuts :

- $Q_e \cos\theta_{\mu^+\mu^-} < -0.8$ where $Q_e$ is the charge of the observed electron (positron) and $\theta_{\mu^+\mu^-}$ the polar angle of the dimuon system;
- $Q_e \cos\theta_{\mathrm{miss}} > 0.8$ where $\theta_{\mathrm{miss}}$ is the polar angle of the missing momentum to the three tracks.

The dimuon invariant mass distribution is shown in Fig. 5 for data and simulation. The signal selection efficiency is $(36 \pm 2)\%$ and the number of expected signal events is estimated as $10.4 \pm 0.5$. The dominant background contribution comes from the four-fermion events not included in the signal definition ($1.8 \pm 0.3$), $\mu^+\mu^-$ ($0.4 \pm 0.1$), and, with a lower rate, WW and $\tau^+\tau^-$ events. The total number of expected background events is $2.6 \pm 0.3$. A total of 16 events is found in the data.

### 5.1.2 Hadronic events

The Zee events with a hadronic Z decay are characterized by an isolated electron and a large energy-flow-object multiplicity. Events are preselected by requiring at least five tracks. The electron candidate is chosen as the particle with the largest isolation angle among all the identified electrons, where the isolation angle $\phi_e$ is defined as the angle with respect to the closest track with a momentum greater than $1\,\mathrm{GeV}/c$. The electron (positron) candidate must fulfil the kinematic requirements of the signal definition and its isolation angle must satisfy $\cos\phi_e < 0.8$. The invariant mass of the rest of the event must be greater than $50\,\mathrm{GeV}/c^2$ and the cosine of the angle of its momentum with respect to the electron (positron) beam direction must be greater than 0.85. The missing momentum is required to be at least $20\,\mathrm{GeV}/c$ and the missing energy has to exceed 50% of the beam energy. The remaining energy-flow objects are clustered into two jets with the `DURHAM` algorithm [14]. The dijet opening angle must be greater than $60^\circ$.

The hadronic invariant mass distribution for data is shown in Fig. 6 after all the selection requirements except the invariant mass cut and is compared with the simulated signal and background events. The average efficiency is $(23.2 \pm 0.4)\%$. The breakdown of the numbers of events selected and the signal and background events expected are listed in

Table 7. The $q\bar{q}$ events represent about half of the background; the rest is split between ZZ (40%) and WW events (10%). A total of 111 events is selected with an estimated background contribution of $22.4 \pm 0.7$ events.

Table 7: Number of selected events for hadronic single-Z selection and expected background contamination for each CM energy. The quoted errors are due to the finite statistics of the simulation.

| Energy (GeV) | Selected events | Expected signal | Expected background |
|---|---|---|---|
| 183 | 5 | $6.4 \pm 0.3$ | $1.6 \pm 0.1$ |
| 189 | 23 | $20.5 \pm 1.0$ | $6.8 \pm 0.4$ |
| 192 | 5 | $3.6 \pm 0.2$ | $0.9 \pm 0.1$ |
| 196 | 15 | $10.0 \pm 0.5$ | $2.2 \pm 0.2$ |
| 200 | 14 | $10.9 \pm 0.5$ | $2.5 \pm 0.2$ |
| 202 | 10 | $5.9 \pm 0.3$ | $1.2 \pm 0.1$ |
| 205 | 11 | $12.6 \pm 0.5$ | $2.2 \pm 0.2$ |
| 207 | 28 | $19.8 \pm 0.9$ | $4.9 \pm 0.5$ |
| Total | 111 | $89.9 \pm 1.6$ | $22.4 \pm 0.7$ |

## 5.2 Cross-section measurement

### 5.2.1 Dimuon cross section

The measured cross section of the Zee process with $Z \to \mu^+\mu^-$, is averaged over all CM energies and amounts to

$$\sigma_{\mu\mu} = 55 \pm 16(\text{stat.}) \pm 3(\text{syst.})\,\text{fb}$$

to be compared to the prediction of the `WPHACT` generator $(44 \pm 2)$fb [15]. The systematic uncertainty is dominated by the statistical uncertainty of the estimated efficiency and corresponds to $\pm 3$ fb. The systematic uncertainty due to the background contamination estimate is $\pm 1$ fb. The luminosity determination and the lepton identification yield negligible uncertainties ($<1$ fb).

### 5.2.2 Hadronic cross section

The systematic uncertainties related to detector simulation, luminosity determination and hadronization are estimated as in Ref. [5]. The other sources are detailed below and a summary is given in Table 8.

#### Simulated statistics

The finite simulated statistics affect the estimate of the signal efficiency and the background rate. The related uncertainties are typically 24 fb for the signal and 10 fb for the background at each CM energy.

### Background contamination

The uncertainty on the non-WW-like four-fermion background rate is estimated by comparing the predictions of two different generators, `PYTHIA` and `KoralW`. Other backgrounds are treated as in Section 4.

### Lepton identification and isolation cut

According to the studies of Ref. [5], a 1% uncertainty is assigned to the lepton identification efficiency. A comparison of the $\phi_e$ distributions in the data and the simulation of WW semileptonic events yields a 1% uncertainty on the corresponding efficiency for single-Z events.

Table 8: Single-Z hadronic cross section systematic uncertainties, at each CM energy.

| Source | Relative uncertainty in % |
|---|---|
| Generator-dependent efficiency | 2.0 |
| Simulated statistics | 4.7 |
| Detector simulation | 0.9 |
| Background contamination | 1.1 |
| Luminosity determination | 0.5 |
| Hadronization | 0.5 |
| Lepton identification | 1.0 |
| Isolation cut | 1.0 |
| Total | 5.5 |

The cross-section measured values for the hadronic single-Z process are shown in Table 9 and Fig. 7 for each CM energy, together with a comparison to the theoretical expectations from `GRC4F`.

Table 9: Measured single-Z cross section and expected uncertainty for each CM energy. In the second column, the ratio between the measured cross section and that predicted by `GRC4F` ($R_Z$) is given.

| Energy (GeV) | $\sigma \pm$ stat. $\pm$ syst. (pb) | $R_Z \pm$ stat. $\pm$ syst. |
|---|---|---|
| 183 | $0.27 \pm 0.20 \pm 0.03$ | $0.52 \pm 0.40 \pm 0.06$ |
| 189 | $0.42 \pm 0.12 \pm 0.03$ | $0.78 \pm 0.22 \pm 0.06$ |
| 192 | $0.61 \pm 0.29 \pm 0.03$ | $1.11 \pm 0.52 \pm 0.05$ |
| 196 | $0.72 \pm 0.18 \pm 0.03$ | $1.27 \pm 0.31 \pm 0.05$ |
| 200 | $0.59 \pm 0.17 \pm 0.03$ | $1.02 \pm 0.29 \pm 0.05$ |
| 202 | $0.89 \pm 0.24 \pm 0.03$ | $1.50 \pm 0.41 \pm 0.05$ |
| 205 | $0.42 \pm 0.17 \pm 0.03$ | $0.69 \pm 0.28 \pm 0.05$ |
| 207 | $0.70 \pm 0.13 \pm 0.03$ | $1.15 \pm 0.22 \pm 0.05$ |

The average hadronic cross section is :

$$\sigma = 0.56 \pm 0.05(\text{stat.}) \pm 0.02(\text{syst.})\,\text{pb}.$$

The average ratio between the measured cross section and that predicted by GRC4F is :

$$\mathrm{R_Z} = 0.98 \pm 0.10(\text{stat.}) \pm 0.03(\text{syst.})$$

As a cross-check, the same ratio was computed with WPHACT and amounts to $0.98 \pm 0.11(\text{stat.}) \pm 0.03(\text{syst.})$.

# 6 Conclusions

The single-W cross section has been measured with the ALEPH detector at eight CM energies from 183 to 209 GeV. The ratio between the measured and the GRC4F predicted cross section averaged over all CM energies is :

$$\mathrm{R_W} = 0.96 \pm 0.11(\text{stat.}) \pm 0.04(\text{syst.}) \pm 0.05(\text{theory}).$$

This result supersedes the previous ALEPH single-W measurement [16] obtained with data collected in 1996 and 1997.

The cross sections of the Zee process in the dimuon and in the hadronic final states at each CM energy between 183 and 209 GeV have been determined. In the $\mathrm{Z} \to \mu^+\mu^-$ channel, the average cross section is :

$$\sigma_{\mu\mu} = 55 \pm 16(\text{stat.}) \pm 3(\text{syst.})\,\text{fb},$$

in agreement with the Standard Model prediction of $(44 \pm 2)$ fb from WPHACT.

The single-Z cross section in the hadronic final states is determined for each CM energy. The average ratio between the measured cross section and the predicted GRC4F value is :

$$\mathrm{R_Z} = 0.98 \pm 0.10(\text{stat.}) \pm 0.03(\text{syst.}) \pm 0.05(\text{theory}).$$

No deviation from the Standard Model expectation is observed for single-W and single-Z production rates. Similar results have been published by other LEP experiments for single-W [17, 18] and single-Z [17, 19, 20] production.

# Acknowledgements

We would like to thank Y. Kurihara, M. Skrzypek and Z. Wąs for invaluable discussions. We wish to thank our colleagues from the accelerator divisions for the successful operation of LEP. It is also a pleasure to thank the engineers and technicians of the collaborating institutions for their support in constructing and maintaining the ALEPH experiment. Those of us from non-member states thank CERN for its hospitality.

# References


[1] K. Hagiwara *et al.*, Nucl. Phys. **B365** (1991) 544.

[2] T. Tsukamoto and Y. Kurihara, Phys. Lett. **B389** (1996) 162.

[3] ALEPH Collaboration, *ALEPH: a detector electron-positron annihilations at LEP*, Nucl. Instrum. and Methods **A294** (1990) 121.

[4] ALEPH Collaboration, *Performance of the ALEPH detector at LEP*, Nucl. Instrum. and Methods **A360** (1995) 481.

[5] ALEPH Collaboration, *Measurement of W-pair production in $e^+e^-$ collisions at centre-of-mass energies from 183 to 209 GeV*, CERN-PH-EP/2004-012, to be published in Eur. Phys. J. C.

[6] ALEPH Collaboration, *Measurement of the absolute luminosity with the ALEPH detector*, Z. Phys. **C53** (1992) 375.

[7] D. Bederede *et al.*, *SICAL - a high precision silicon-tungsten calorimeter for ALEPH*, Nucl. Instrum. and Methods **A365** (1995) 117.

[8] *Reports of the Working Groups on Precision Calculations for LEP2 physics*, edited by S. Jadach, G. Passarino and R. Pittau (CERN 2000-009, Geneva, 2000).

[9] S. Jadach *et al.*, Comput. Phys. Commun. **140** (2001) 475; Weights described in S. Jadach *et al.*, Eur. Phys. J. **C27** (2003) 19, were applied to single-W events.

[10] J. Fujimoto *et al.*, Comput. Phys. Commun. **100** (1997) 128.

[11] T. Sjöstrand *et al.*, Comput. Phys. Commun. **135** (2001) 238.

[12] W. Bartel *et al.*, Z. Phys. **C33** (1986) 23;
S. Bethke *et al.*, Phys. Lett. **B213** (1988) 235.

[13] ALEPH Collaboration, *Searches for new particles with the ALEPH detector*, Phys. Rep. **216** (1992) 275.

[14] Yu. L. Dokshitzer, J. Phys. **G17** (1991) 1441.

[15] E. Accomando and A. Ballestrero, Comp. Phys. Commun **99** (1997) 270;
E. Accomando, A. Ballestrero and E. Maina, Comp. Phys. Commun **150** (2003) 166.

[16] ALEPH Collaboration, *A study of Single W Production in $e^+e^-$ Collisions at $\sqrt{s}$=161-183 GeV*, Phys. Lett. **B462** (1999) 389.

[17] DELPHI Collaboration, *Single intermediate vector boson production in $e^+e^-$ collisions at $\sqrt{s}$=183 and 189 GeV*, Phys. Lett. **B515** (2001) 238.

[18] L3 Collaboration, *Production of single W bosons in $e^+e^-$ interactions at $130 \leq \sqrt{s} \leq 183\,GeV$ and limits on anomalous $WW\gamma$ couplings*, Phys. Lett. **B436** (1998) 417;
L3 Collaboration, *Production of single W bosons in $e^+e^-$ interactions at $\sqrt{s}$=189 GeV and limits on anomalous $WW\gamma$ couplings*, Phys. Lett. **B487** (2000) 229;
L3 Collaboration, *Production of single W bosons at LEP and measurement of $WW\gamma$ gauge coupling parameters*, Phys. Lett. **B547** (2002) 151.

[19] L3 Collaboration, *Study of $e^+e^- \to Ze^+e^-$ process at LEP*, Phys. Lett. **B561** (2003) 73.

[20] OPAL Collaboration, *First measurement of $Z/\gamma^*$ production in Compton scattering of quasi-real photons*, Phys. Lett. **B438** (1998) 391;
OPAL Collaboration, *Measurement of $Z/\gamma^*$ production in compton scattering of quasi-real photons*, Eur. Phys J. **C24** (2002) 1.

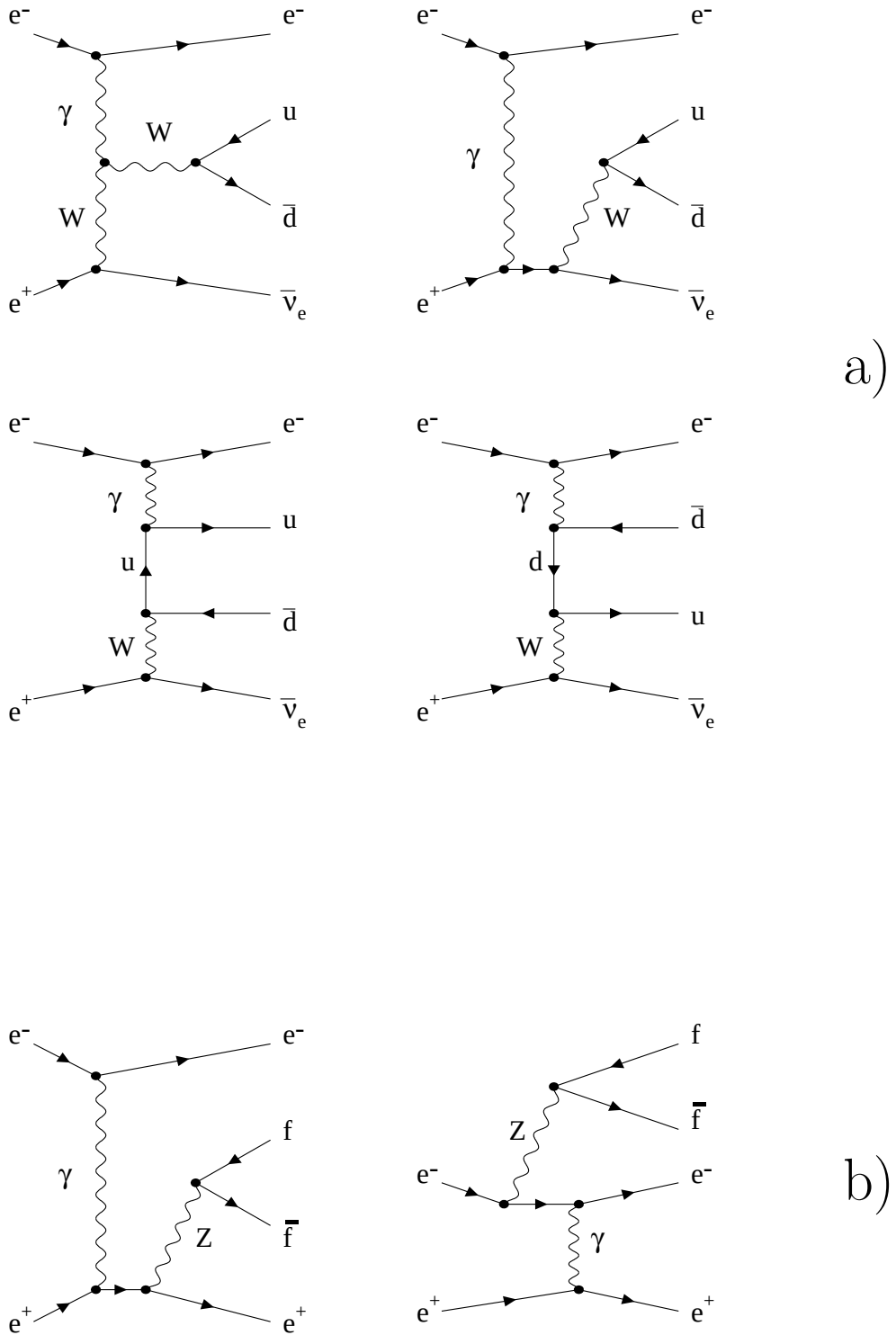


Figure 1: Dominant diagrams for a) hadronic single-W final state, b) single-Z processes.

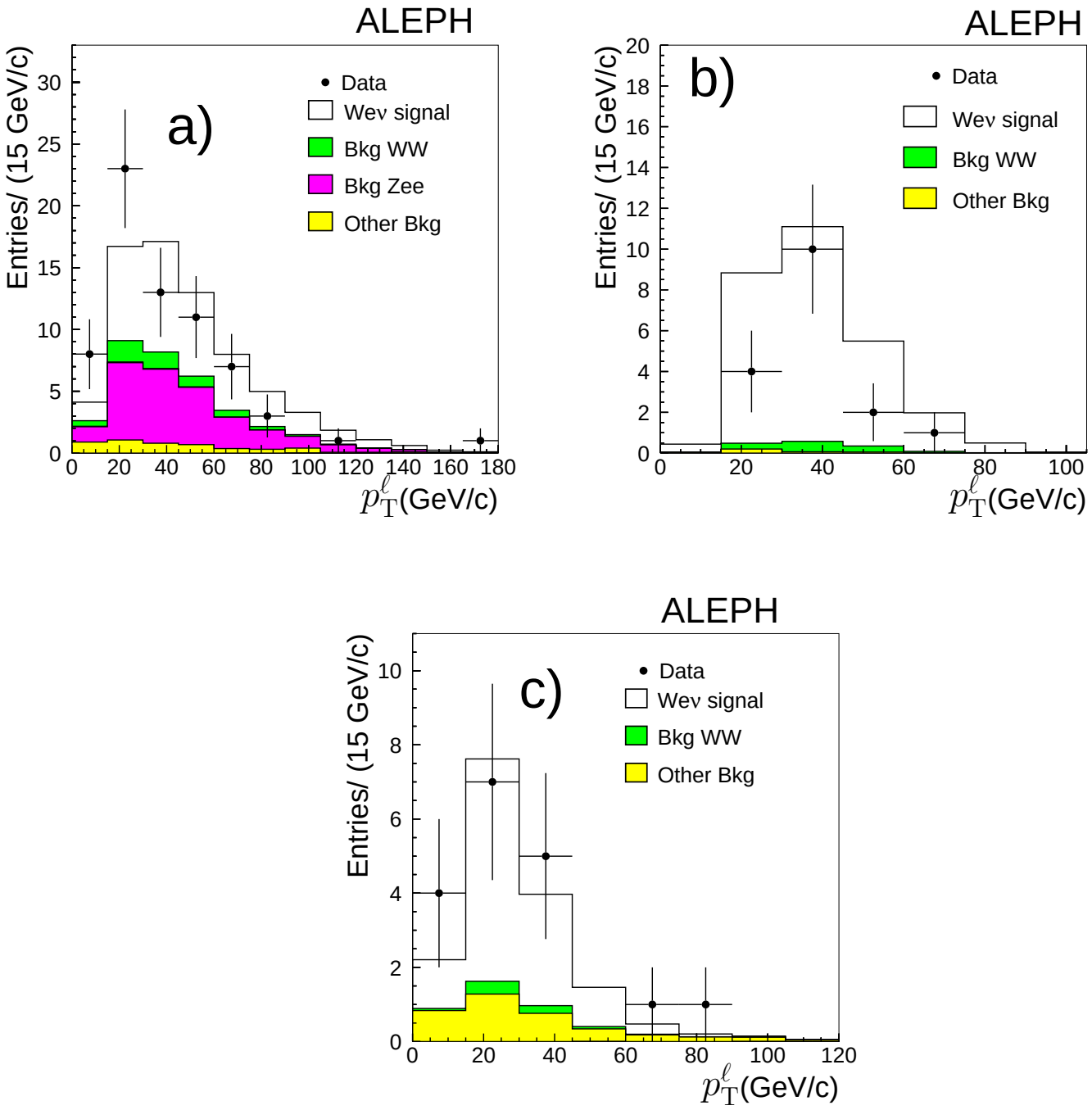


Figure 2: Distributions of the lepton transverse momentum ($p_T^\ell$) for the three single-W leptonic channels: a) W$\rightarrow e\nu$, b) W$\rightarrow \mu\nu$, and c) W$\rightarrow \tau\nu$, in the data (points with error bars) and in the simulation (signal: empty histogram, background: shaded histograms) for all CM energies.

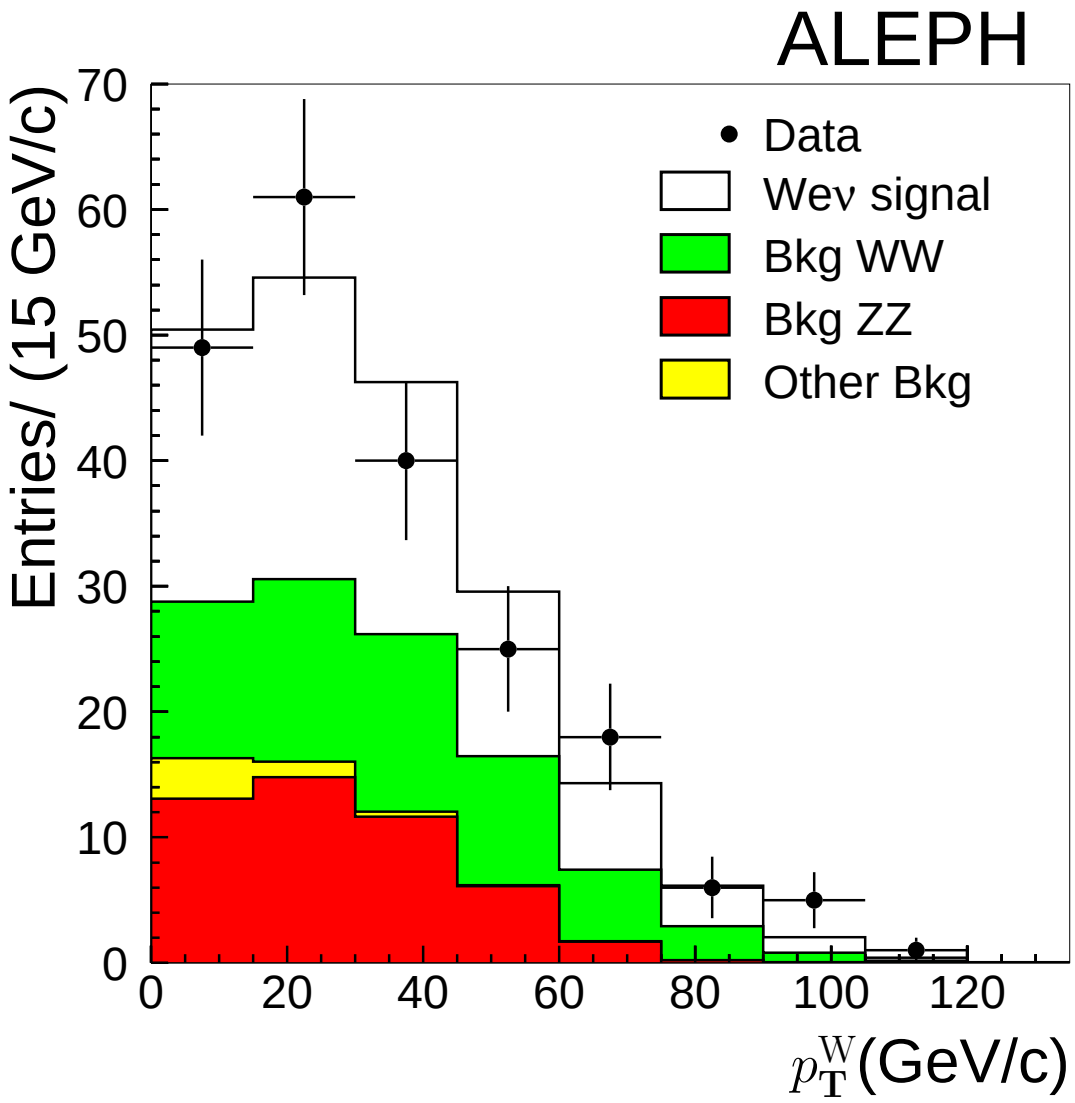


Figure 3: Distribution of the reconstructed W transverse momentum ($p_{\mathrm{T}}^{\mathrm{W}}$) for the single-W hadronic channel, in the data (points with error bars) and in the simulation (signal: empty histogram, background: shaded histograms) for all CM energies.

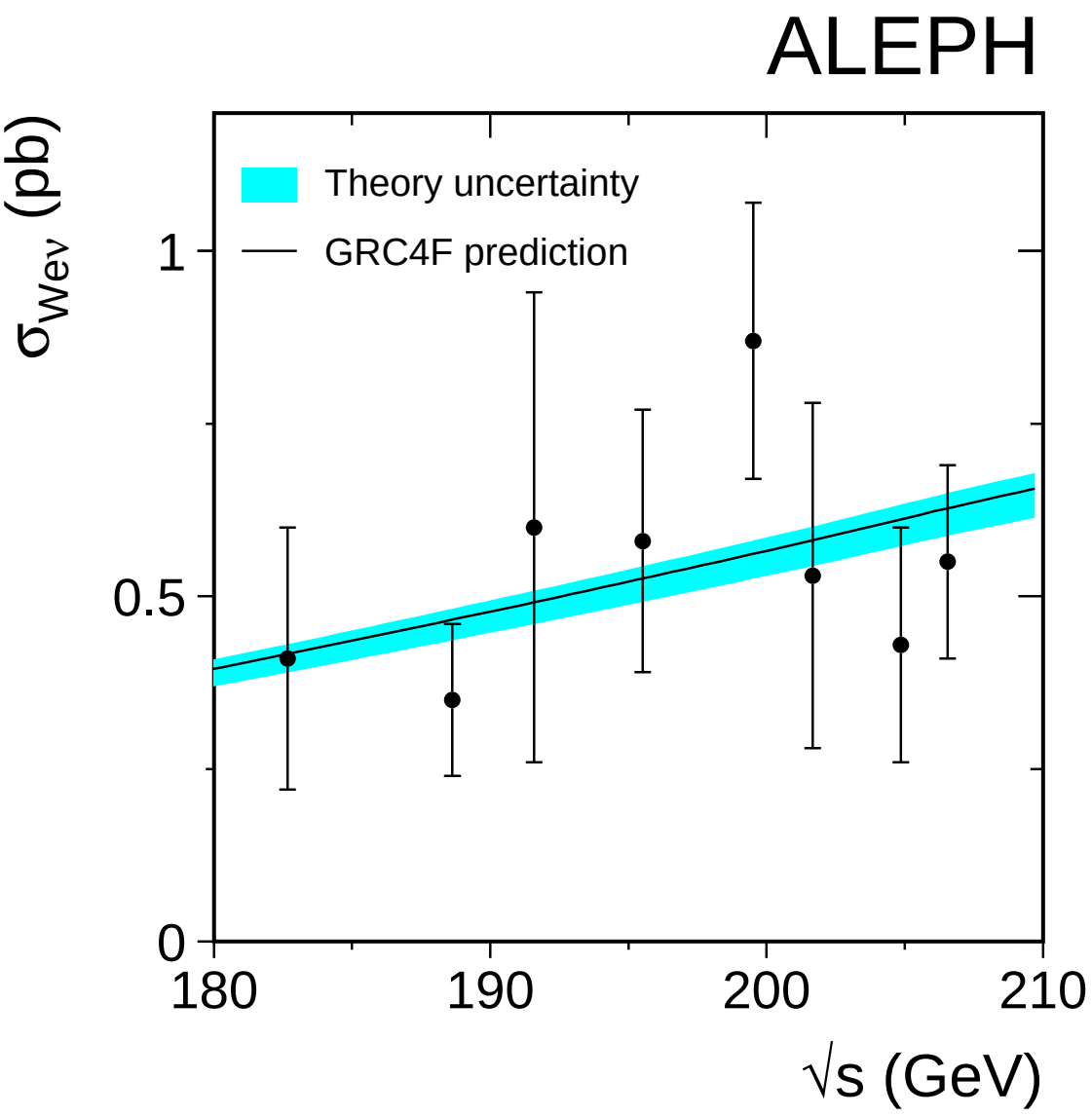


Figure 4: Measured single-W cross section as a function of the CM energy. The solid line shows the expected cross section from the GRC4F generator. The uncertainty on the theoretical cross section is represented by the shaded band.

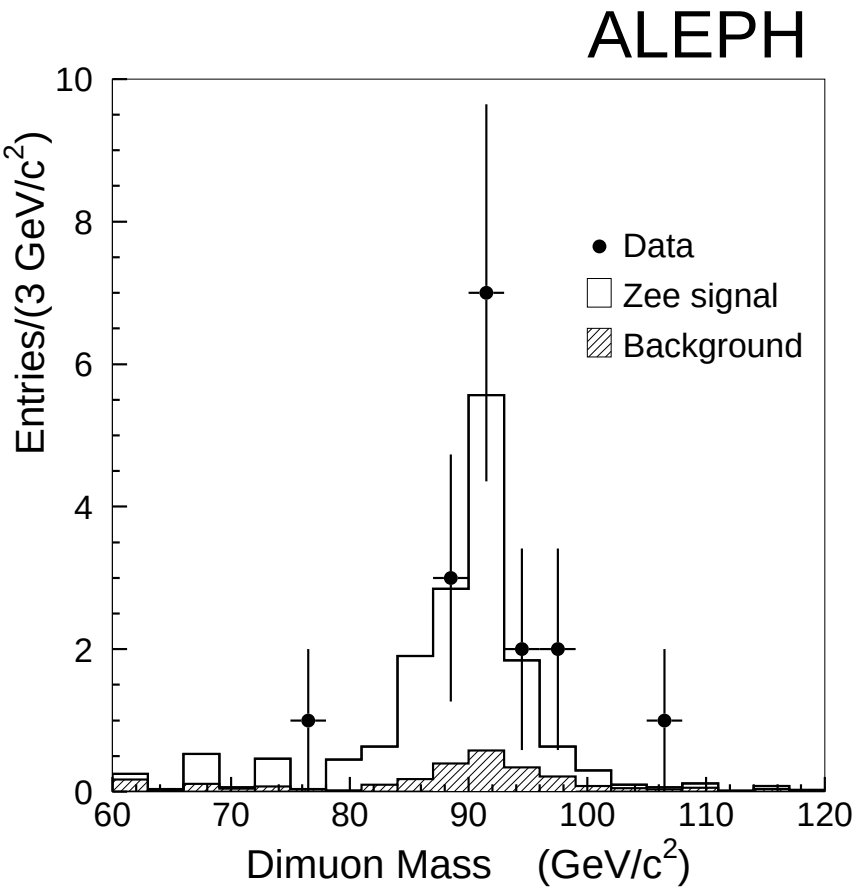


Figure 5: Dimuon invariant mass distribution after the muonic single-Z selection, in the data (points with error bars) and the simulation (signal: empty histogram, background: shaded histogram), for all CM energies.

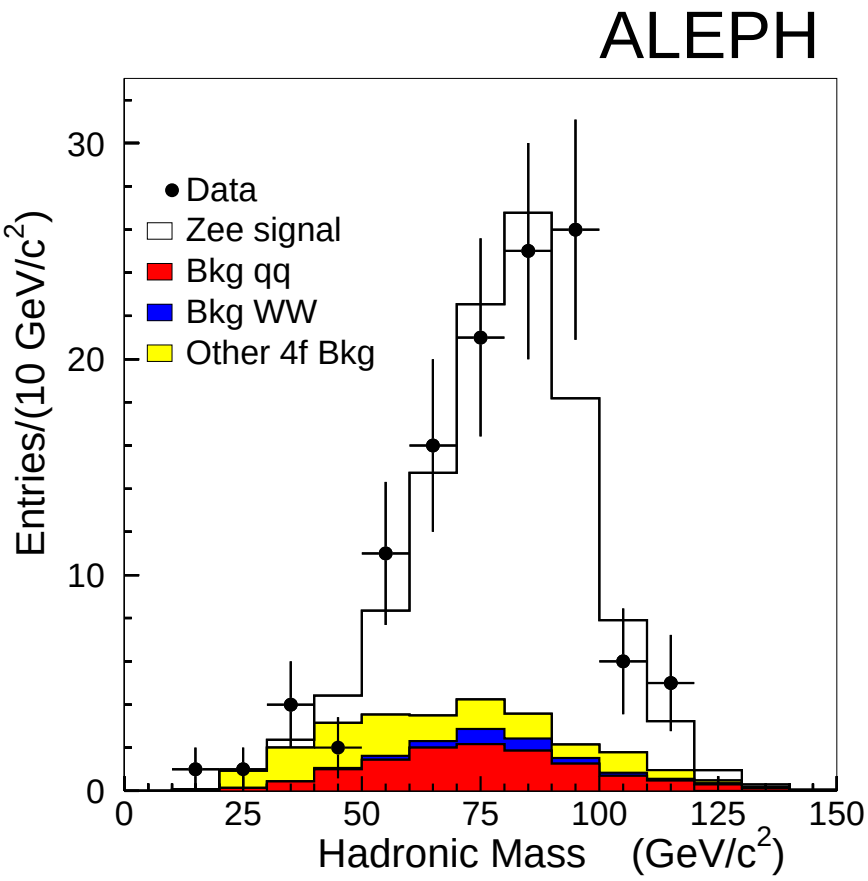


Figure 6: Invariant mass distribution of the hadronic system after the hadronic single-Z selection, in the data (points with error bars) and the simulation (signal: empty histogram, background: shaded histograms) for all CM energies.

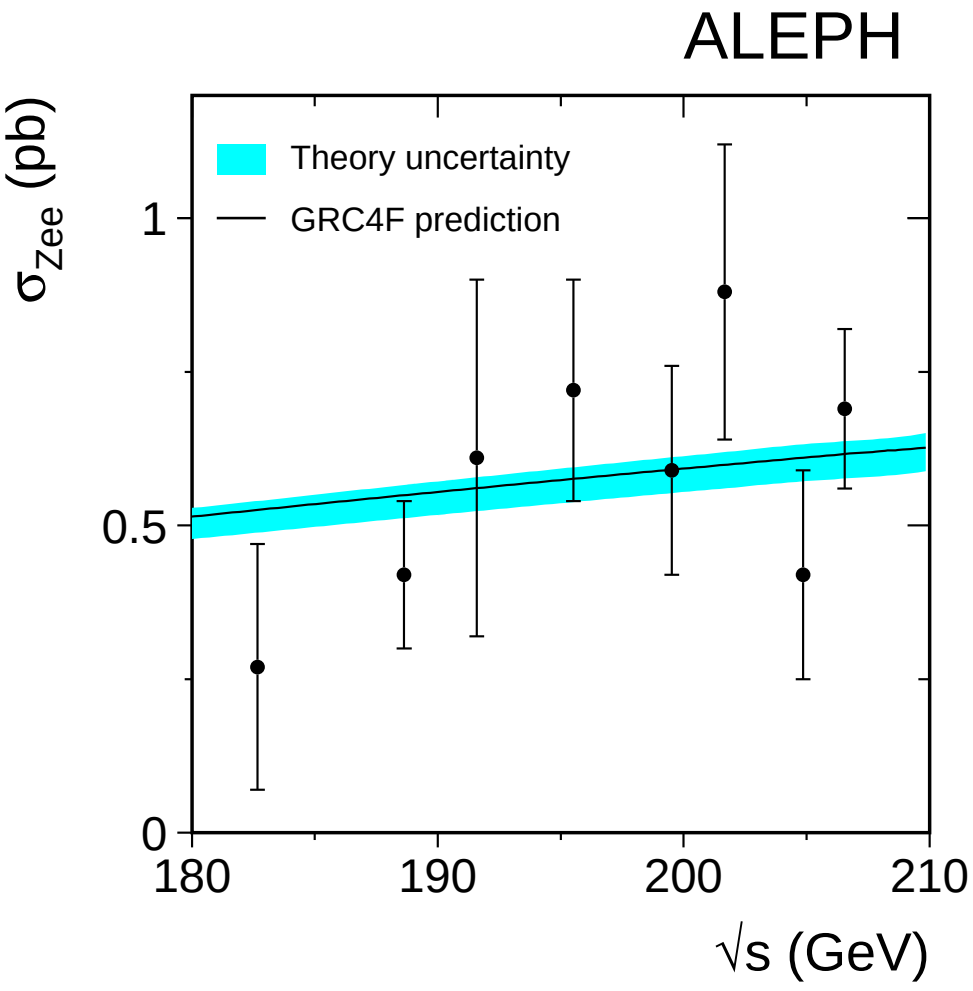


Figure 7: Measured single-Z cross section as a function of the CM energy. The solid line shows the expected cross section from the GRC4F generator. The uncertainty on the theoretical cross section is represented by the shaded band.